Gellan gum/bacterial cellulose hydrogel crosslinked with citric acid as an eco-friendly green adsorbent for safranin and crystal violet dye removal

Gellan gum/bacterial cellulose hydrogel crosslinked with citric acid as an eco-friendly green adsorbent for safranin and crystal violet dye removal

Hau Trung Nguyen[1], Fahanwi Asabuwa Ngwabebhoh[1,2], Nabanita Saha*[1,2,3], Tomas Saha[2], Petr Saha[1,2,3]

[1]Centre of Polymer Systems, University Institute, Tomas Bata University in Zlin, Trida Tomase Bati 5678, 76001 Zlin, Czech Republic

[2]Footwear Research Centre, University Institute, Tomas Bata University in Zlin, Nad Ovcirnou IV, 3685, Zlin, Czech Republic

[3]Faculty of Technology, Tomas Bata University in Zlin, Vavrečkova 275, 76001 Zlin, Czech Republic

Abstract

In this study, ex-situ crosslinked gellan gum (GG)/bacterial cellulose (BC) hydrogels have been investigated as good absorbents for the removal of safranin and crystal violet dye pollutants. The preparation involves a cost-effective and easy-to-perform crosslinking procedure, using citric acid (CA) as a green crosslinker. The physicochemical and mechanical properties of the crosslinked hydrogels were examined by FTIR, TGA, SEM, XRD, and unconfined compression analyses. The swelling capacity of the hydrogels as a function of pH was investigated. CA depicted to improve structural stability as a crosslinker. The dye removal capacity of the hydrogels as good adsorbents was explored and showed higher efficiency in the removal of safranin dye as compared to crystal violet with optimum adsorption capacities obtained as 17.57 and 13.49 mg/g, respectively. Adsorption kinetics and isotherm models as well as thermodynamics examined. Results showed the adsorption process well fitted the pseudo 2nd-order kinetic and Langmuir-Freundlich models while temperature dependence study depicted to be exothermic. Furthermore, no significant loss of removal efficiency of the hydrogel adsorbent was observed even after five adsorption-desorption cycles. Based on the revealed results, the prepared hydrogel may serve as an effective adsorbent for the removal of dyes from the aqueous phase.

Keywords: Hydrogel, Green crosslinking, Bacterial cellulose, Gellan gum, Dye removal, Adsorption modeling

*Corresponding author:
Email address: nabanita@utb.cz (N. Saha)

1. Introduction

In recent years, pollution growth attributed to rapid urbanization has led to an increase in industrial effluent discharge containing pollutants such as heavy metals, textile dyes, tanning bleaches, pesticides, and detergents in our environment [1-3]. This has attracted great attention due to its potential threat to human health and ecological balance. Among all, textile effluents especially dye present one of the highest environmental pollutants. Therefore, the need to decontaminate such pollutants is of high priority to maintain ecological balance and biodiversity with reduced negative effects on biological cycles [4-6].

Various techniques have been developed and applied for the removal of dye pollutants from wastewater, which include coagulation, oxidation, ultrafiltration, reverse osmosis, flocculation, precipitation, adsorption, and catalytic degradation [4, 6-8]. Among these, adsorption is considered to be one of the simplest methods since it is less expensive and easy to adapt for potential industrial applications [9-12]. But certain limitations like the expensive cost of the synthesis of the adsorbents hamper large-scale usage [3]. However, more economical alternative adsorbents have been continuously explored and developed, such as carbon nanotubes, metal-organic frames, clay, activated carbon, and hydrogels [1-3, 11, 13, 14]. Hydrogel-based adsorbents, especially from natural polymers, have proven promising due to their outstanding features including abundant raw materials, low cost, sustainability, and ease in functionalization.

Gellan gum (GG) a biopolymer produced by *Pseudomonas elodea*, possesses high commercial potential and contains several hydrophilic groups in its molecular structure [15-18]. However, pure GG hydrogels are weak with low mechanical integrity but modified with other polymers to enhance functionalities including improved thermal stability and adsorption properties [19-21]. Bacterial cellulose (BC) has also proven to be a well-suited absorbent [1, 2, 9, 21]. This biopolymer has revealed improved adsorption efficiency towards a wide variety of contaminants, especially dyes and metal ions [1, 21, 22], which is due to the presence of many hydroxyl groups on its backbone. In order to improve the material properties, various crosslinkers have been explored to increase mechanical stability but there exist issues of water solubility and toxicity related to the crosslinkers used. BC modification has been mostly applied via ex-situ and in-situ methods to enhance its properties by incorporation of active functional groups in/on its structure/surface [2, 23, 24]. Nevertheless, the ex-situ modification has proven more versatile and simpler than the in-

situ method due to its non-toxicity to the BC structure and properties, especially during biosynthesis [25, 26] . Moreover, ex-situ modification on pristine BC has been well achieved by impregnation, lamination, or blending with different materials, mainly through graft copolymerization or crosslinking reactions [21, 23]. From the point of view of product development, crosslinking reactions have been explored to modify numerous biopolymers. Although various crosslinkers provide improved mechanical stability and compatibility to the polymer matrices, there exist issues with water solubility and toxicity [27]. Amongst all, citric acid (CA) has been applied as a green crosslinker and showed enhancement in mechanical property and water stability for different biopolymer matrices to form hydrogels and biocomposites [28-31].

The use of CA as a promising crosslinker is not limited only to its safety and non-toxicity, but also because it forms stable crosslinking bonds with polymers containing a high density of hydroxyl groups [32-34]. Moreover, CA is easily accessible and economical, making it commercially attractive [32, 33, 35]. Herein, to develop an eco-friendly biopolymer-based hydrogel adsorbent, GG and BC were crosslinked with CA as a green crosslinker. To the best of our knowledge, this is the first report relating to the crosslinking of BC-supported GG with CA to form a stable hydrogel system. The prepared crosslinked hydrogels were characterized based on surface morphology, thermal stability, and mechanical integrity. The hydrogel was further used as green adsorbents for selected SO and CV water dye pollutants. The dye removal capacity of the hydrogel was studied and the adsorption kinetics, isotherm, and thermodynamics were evaluated. In addition, the reusability efficiency of the prepared hydrogel adsorbent was investigated for n-cycles.

2. Materials and Methods

2.1. Materials

Bacterial cellulose (BC) was prepared at our laboratory at Tomas Bata University in Zlin. Gellan gum (GG, low acyl gellan), polyethylene glycol 3000 (PEG), crystal violet ($C_{25}N_3H_{30}Cl$, purity ≥90%), safranin O ($C_{20}H_{19}N_3N_4Cl$, purity ≥85%) and sodium hydroxide (NaOH) were supplied by Sigma-Aldrich (Darmstadt, Germany). Citric acid (CA, $C_6H_8O_7$) as green crosslinker and hydrochloric acid (HCl) were purchased from Penta s.r.o. (Zlin, Czech Republic). The reagents were of analytical grade with high purity and were used without further purification. Distilled

water was used for the preparation of all aqueous solutions. Waste whey was collected from Kromilk A.S (Kromeriz, Czech Republic). Black tea was purchased from a grocery store in Zlin, Czech Republic. Sucrose was supplied by Amersco LLC (MA, USA). All reagents were used without further purification.

2.2. Culture and treatment of bacterial cellulose

BC was produced as described in our previous studies [36, 37]. In brief, sour whey waste, black tea, and sucrose were directly mixed, and sterilized at 121 °C under 1 atm for 15 min. By a fermentation method using *Komagatacibacter xylinus* CCM 3611, the mixture was incubated under static culture conditions for 15 days at 30 °C. Thereafter, the formed BC membranes were harvested and treated by immersion in 0.5 %w/v NaOH at 80 °C for 2 h, followed by triplicate washing with distilled water (dH_2O) and blended vigorously at 30000 rpm for 2 min using a NutriBullet® blender (N17-0908 machine, USA). The BC solution was then determined based on its dry weight percentage by freeze-drying.

2.3. Preparation of gellan gum-bacterial cellulose (GB) hydrogels

The hydrogels were prepared by mixing different components at varying ratios as calculated in terms of weight percent (%w/w) shown in Table 1. Initially, GG and PEG were completely dissolved in dH_2O at 80 °C for 1 h. BC was then added under continuous stirring. The obtained homogenous mixtures were allowed to cool down and immersed in CA. The samples were kept at 30 °C overnight followed by treatment at 85 °C for 90 min. The crosslinked hydrogel samples were collected, washed several times with dH_2O, freeze-dried at -110 °C, and stored in a desiccator for further use. The obtained hydrogels were denoted as GB and assigned as GB0, GB1, GB2, GB3, GB4 and GB5 following the different formulated compositions as shown in Table 1.

Table 1.
Components of GB hydrogel.

Samples	GG (%w/v)	BC (%w/v)	PEG (%w/v)	CA (%w/v)
GB0	1	0.5	/	/
GB1	0.5	0.5	10	10
GB2	1	0.5	10	10
GB3	2	0.5	10	10
GB4	1	0.5	10	5
GB5	1	0.5	10	15

2.4. Swelling study and point zero charge determination of hydrogel

The swelling capacities of the GB hydrogels were performed to evaluate their water retention ability. Prior to analysis, the prepared dried samples were initially weighed (S_1) followed by complete immersion in 0.1M phosphate-buffered saline (PBS) solutions of varying pH (3, 5, 7, 9 and 11) and equilibrated for 24 h. The swollen samples were collected from the swelling medium, blotted with tissue paper to remove excess water and weighed (S_2). The results were recorded in triplicates and the average value was calculated. The swelling ratio percentages (SR%) of the prepared GB hydrogels were then determined using Eq. 1 [38, 39].

$$\mathrm{SR\%} = \frac{S_2 - S_1}{S_1} \times 100 \quad (1)$$

The point zero charge (PZC) of the GB hydrogel was determined by immersing 0.2 g of the hydrogel in 10 mL of dH_2O at different pH ranging from 3–11 for 24 h. The initial and final pH of the solutions was determined by an electronic handheld pH meter (Lovibond pH meter-445R, USA), and their PZC was calculated by using the equation $\Delta pH = pH_{initial} - pH_{final}$.

2.5. Characterization of GB hydrogels

Surface morphology of the GB hydrogels was examined under a scanning electron microscope (SEM) (FEI™, Brno, Czech Republic) at an accelerating voltage of 5 kV. Fourier Transformed Infrared Spectroscopy (FT-IR) was performed using a Nicolet iS5 (Thermo Scientific, Waltham, MA, USA) spectrometer in the range of 400-4000 cm^{-1}. Thermal degradation was analyzed using a TGA Q500 (TA Instruments, USA) by heating from 25 to 600 °C under a nitrogen atmosphere at a heating/cooling rate of 10 °C/min. The degree of crystallinity was analyzed by X-ray diffraction (XRD) using a Mini Flex™ 600 X-ray diffractometer (Rigaku, Japan) in the range of 5 - 60°. Mechanical properties were analyzed under unconfined compression on a uniaxial Instron 5567 testing machine (Instron, Norwood, MA, USA) with a static load of 5 kg at a compression rate of 1 mm/min and at room temperature using swollen samples of 20 mm in diameter.

2.6. Adsorption study

The dye adsorption study was performed via single batch reactor systems consisting of 5 independent parameters: effect of contact time (1 – 1440 min), solution pH (3 – 11), initial dye

concentration (1 – 10 mg/L), temperature (25 – 55 °C), and adsorbent dosage (100 – 300 mg). The adsorption capacity of the GB hydrogels was established by measuring the concentrations of CV and SO dyes before and after the test period using a UV-Vis spectrometer (Varian UV-VIS-NIRT, MA, USA) at λ_{max} 590 and 520 nm, respectively. The amount of dye adsorbed at equilibrium and removal percentage (%R) was then determined using Eqs. (2) and (3) [40-43].

$$Q_e = \frac{(C_i - C_e)V}{M} \quad (2)$$

$$\%R = \frac{C_i - C_e}{C_i} \times 100 \quad (3)$$

where, Q_e (µg/g) is the equilibrium adsorbed dye onto GB, C_i (mg/L) is the initial concentration of dyes, C_e (mg/L) is the equilibrium concentrations of dyes in the liquid phase at time, *t*, *V* (L) is the volume of dye solutions and *M* (g) is the mass of GB hydrogels.

2.7. Adsorption kinetics, isotherm modeling and thermodynamics

The rate of adsorption of the different investigated dyes depends on both the contact time of the adsorbent with adsorbates and the diffusion processes. In order to understand the adsorption processes of SO and CV dyes on GB hydrogel, the Pseudo-1st order (Eq. 4), Pseudo-2nd order (Eq. 5), the intraparticle diffusion (Eq. 6) and Boyd kinetic models were applied [42, 44, 45].

$$\log(Q_e - Q_t) = logQ_e - \frac{K_1}{2.303}\, t \quad (4)$$

$$\frac{t}{Q_t} = \frac{1}{K_2 Q_e^2} + \frac{t}{Q_e} \quad (5)$$

$$Q_t = K_3 t^{0.5} + C \quad (6)$$

$$B_t = -0.4977 - \ln(1 - F) \quad (7)$$

Where, Q_e and Q_t (mg/g) represents the adsorption capacities at equilibrium and time, *t*, respectively. K_1 (min^{-1}) is the pseudo-1st order adsorption rate constant, K_2 (g/mg min) is the rate constant of the pseudo-2nd order adsorption process, K_3 (mg/g min$^{0.5}$) is the intraparticle diffusion

rate constant, *C* (mg/g) is the boundary layer effect and *F* is the fraction of dye adsorbed at any time, *t* (min).

Adsorption isotherm models were studied and they describe the interaction between the adsorbent surface and dye molecules at equilibrium. Two parameter isotherm models of Langmuir (Eq. 8) and Freundlich (Eq. 9) model via the non-linear regression method were studied [1, 40, 42, 44, 45]

$$Q_e = \frac{Q_m K_L C_e}{1 + K_L C_e} \tag{8}$$

$$Q_e = K_F C_e^{\frac{1}{n}} \tag{9}$$

Where, Q_m (mg/g) is the maximum adsorption capacity, K_L (L/mg) is the Langmuir constant, K_F (mg/g) (L/mg) is the Freundlich constant, and *n* is the adsorption intensity.

Thermodynamic parameters of change in Gibb's free energy (ΔG°), enthalpy (ΔH°), and entropy (ΔS°) were calculated in order to better understand the effect of temperature on the removal of SO and CV dyes using GB hydrogel adsorbent. This was determined from the linear plot of lnK versus 1/T according, calculated using the Eqs (10), (11) and (12) [41, 44-46].

$$K_d = \frac{C_s}{C_e} \tag{10}$$

$$\Delta G° = -RT ln K_d \tag{11}$$

$$ln K_D = -\frac{\Delta H^o}{RT} + \frac{\Delta S^o}{R} \tag{12}$$

Where, K_d is the equilibrium dissociation constant (a ratio of solid phase to solute concentrations), *R* (8.314 J/mol K) is the universal gas constant, C_s (mg/L) is the concentration of the dye on the adsorbent, and *T* (K) is the temperature.

2.8. Reusability and regeneration study

After dye adsorption, the GB hydrogel adsorbents were immersed in dH_2O at 60 °C for 2 h for the recovery of the dyes. Subsequently, the desorbed hydrogels were regenerated by immersion in 0.1 mol/L aqueous HCl solution for 1 h. The obtained regenerated hydrogels were washed with dH_2O

water to reach neutrality and dried. The adsorption ability of the regenerated hydrogels was performed for 5 cycles and the removal capacity was determined following the protocol previously described in section 2.6 above.

2.9. Statistical analysis

The results are displayed as Mean ± Standard error of mean. Origin Lab software version 9.0 was used for statistical analysis. The experimental data from all the investigations were analyzed using analysis of variance (ANOVA). A value of $p < 0.05$ was determined as statistically significant.

3. Results and discussion

3.1. Preparation of GB hydrogels

The preparation and suggested crosslinking process is illustrated in Figure 1a. According to the literature [47, 48], CA forms a five-member cyclic anhydride intermediate compound at elevated temperature via the integration of its two adjacent carboxyl groups. The intermediate compound then reacts with the hydroxyl groups of GG and BC to form ester bonds. However, crosslinking of the polymer matrix with CA does not significantly contribute to the final mechanical integrity of the material due to acid-catalyzed depolymerization. As a result, PEG was added leading to the formation of both polymer-CA-polymer and polymer-CA-PEG-CA-polymer bonds that occurred at the same time [49]. As such, PEG acted as an intermediate for the bonding between two CA molecules. The addition of PEG increases the number of hydroxyl groups and thus enhances the ex-situ crosslinking, porosity and mechanical stability of the materials. A similar study reported the crosslinking of a cellulose derivative cross-linked with CA and PEG that led to an increase in mechanical and thermal stability of the materials [50].

3.2. Swelling dynamics

Figure 1b presents the swelling capacities in static water at different pH conditions for the prepared GB hydrogels. Overall, all hydrogels showed good swelling abilities attributed to the presence of hydroxyl and carboxylate groups in the gel structure [26, 51]. However, the highest swelling was found for 5% CA GB crosslinked hydrogel as compared to 10%, and 15% CA. These results corroborate the effect of CA is inversely proportional to the swelling of the hydrogels. Considering the higher concentrations of CA (10% and 15%) cause excess crosslinking and limit mobility of

polymer chain thereby resulting in the resistance to expansion of the hydrogel network. Comparatively, a hydrogel without the use of CA and PEG (GB0) as control was prepared and evaluated against the crosslinked hydrogels. The results revealed the highest swelling for GB0 after 24 h, which was approximately 3 times higher than that obtained for GB crosslinked hydrogels. This was attributed to the high hydrophilicity and dominant physical crosslinking (ionic and weak hydrogen bond interaction) existing between GG and BC in GB0, which promoted significant swelling of the hydrogel. Nevertheless, it should be noted that scuh hydrogels with very high swelling related to physical crosslinking sometime show some limitations especially low mechanical stability and easy disintegration in aqueous phase during applications. This in tend limits their performance and reusability. Furthermore, it was clearly seen that all prepared hydrogels exhibited the highest swelling at pH 7. This high swelling property was also observed in the alkaline medium compared to acidic solutions. This phenomenon may be attributed to the high density of negatively charged OH^- and $–COO^-$ groups on the hydrogel structure causing electrostatic repulsions and expansion of the gel network followed by the ease in penetration of water molecules [26, 43, 51].

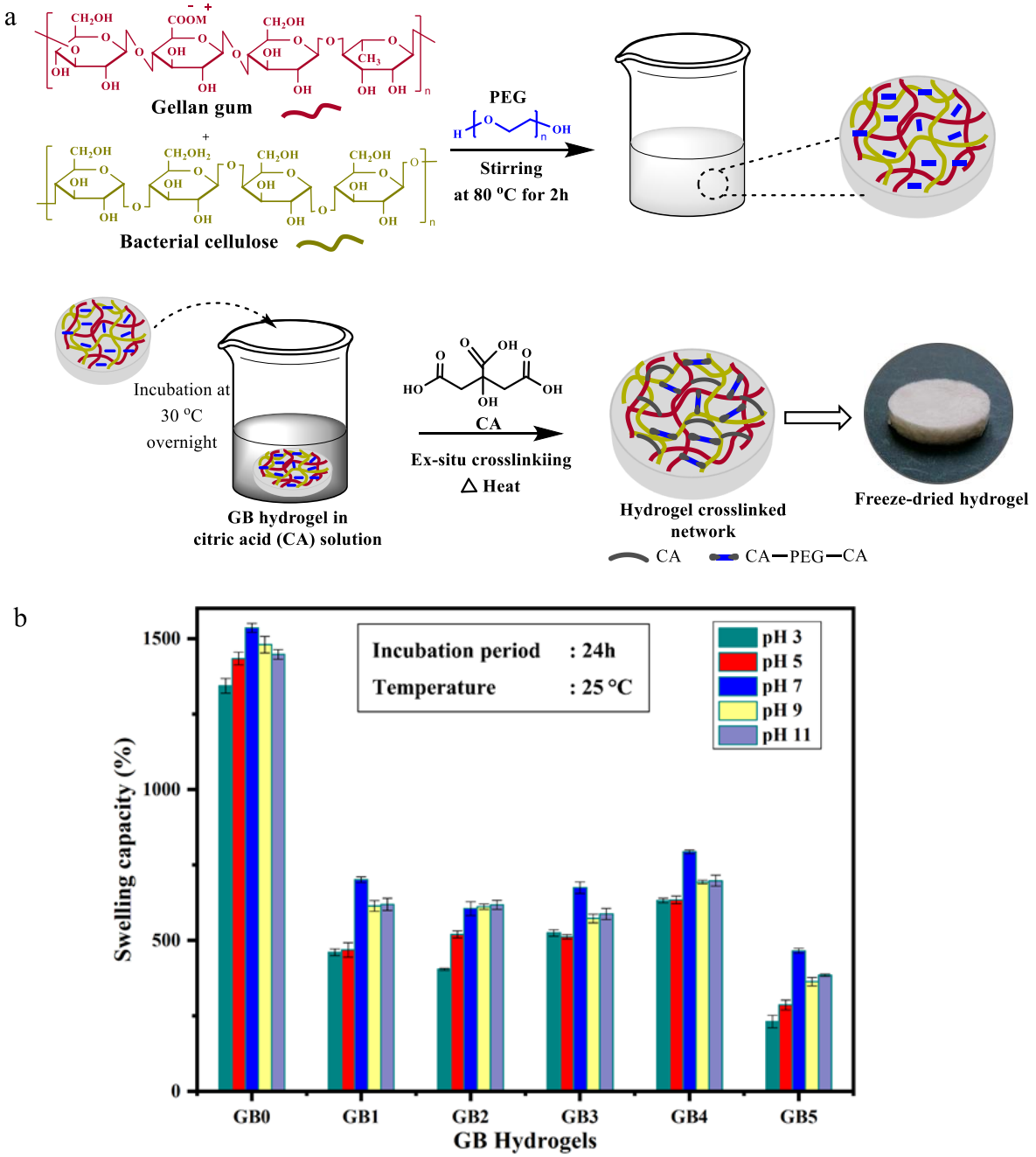

Fig. 1. a) Illustrative steps for the preparation of GB hydrogels. b) Swelling capacity of GB hydrogels in PBS solutions.

3.3. FTIR analysis

The FT-IR spectra of the monomeric components and prepared hydrogels are shown in Figure 2a. As observed, all characteristic bands of GG, BC, PEG, and CA are present in the crosslinked hydrogels (GB1, GB2, GB3, GB4 and GB5). The bands around 3350 are ascribed to OH stretching

vibrations in cellulose and GG backbone. The bands at 2853 and 2908 cm^{-1} relate to the -CH stretching vibration of methoxy and methylene in PEG, cellulose and GG. The bands at around 1602 - 1748 cm^{-1} are due to carbonyl (C=O) stretching from the glycosidic link carboxyl group of GG and CA. This confirmed CA was successfully crosslinked with GG and BC [36, 52]. This could be further confirmed by the absence of the C=O stretching band in the non-crosslinked hydrogel (GB0) as a control. Lastly, the strong band between 1042 - 1099 cm^{-1} and 863 – 905 cm^{-1} observed for all materials was ascribed to C–O–C symmetric stretching [36].

3.4. X-ray diffraction analysis (XRD)

The crystal structure analysis of the prepared hydrogels is displayed in Figure 2b. As observed, the characteristic peaks of cellulose and GG were present in the hydrogels. The two vertices around 2θ angles were determined at ≈14.5° and ≈22.8°, with Miller indices of (100) and (110) corresponding to the characteristic crystal diffraction peaks of pure cellulose structure in BC [36, 37]. The significant peaks around ≈19.3°, 22.0° and 23.4° are represented the presence of GG and PEG in the component of all evaluated hydrogels [53]. The remaining peaks are attributed to the distribution of CA such as the peaks at 17-18°, 26-29°, 30-31.5°, 35-36.3°, and 42.2° [54]. In addition, a slight variation in crystalline behavior between the samples and the pristine components is attributed to the content difference and the pretreatment components process of substrates.

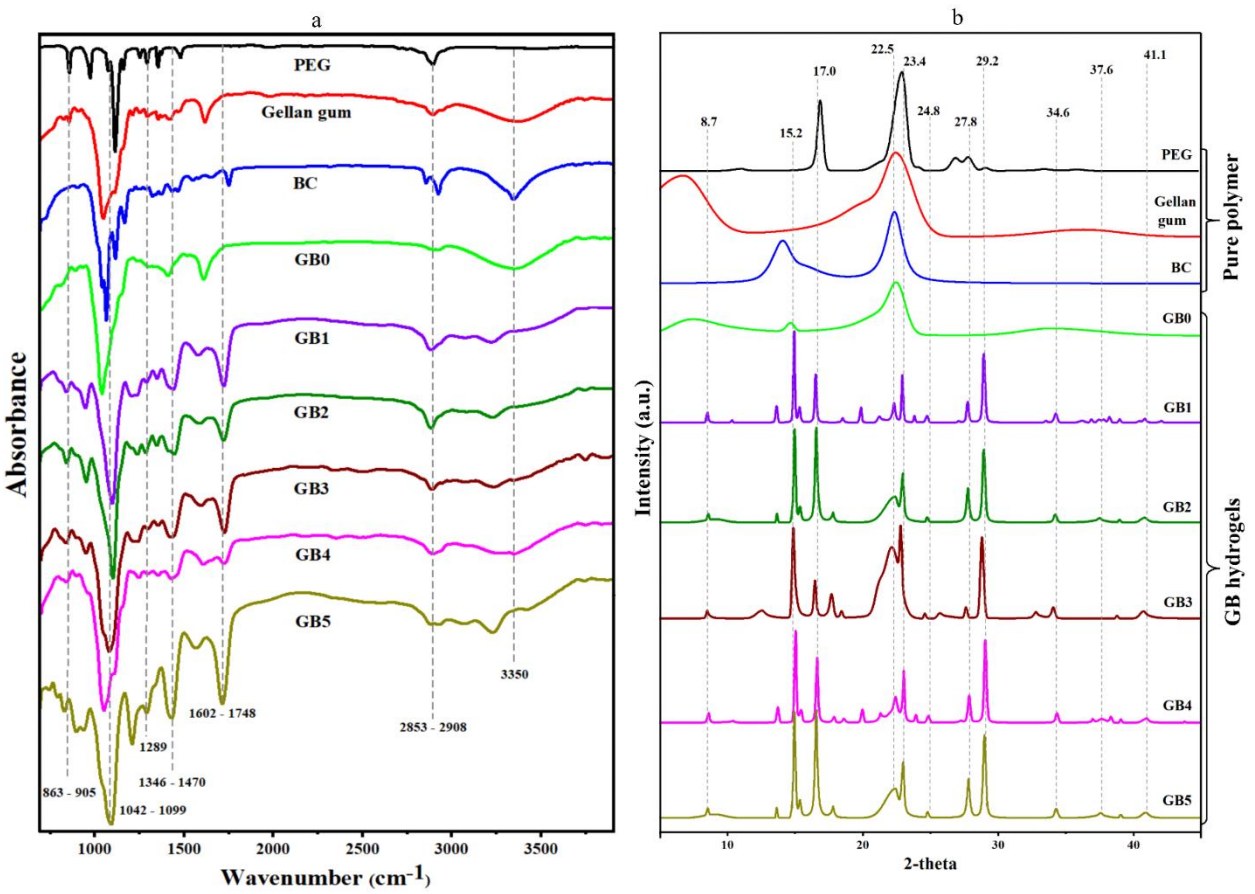

Fig. 2. a) FT-IR spectrum and b) X-ray diffractograms of GB hydrogels and pristine polymers (PEG, Gellan gum, and BC).

3.5. Mechanical properties by unconfined compression test

Unconfined compressibility is an important property with a profound effect on the material's mechanical stability and reusability. Typically, materials that possess high compression modulus show less absorbent efficiency. Figure 3a shows the results of the unconfined compression test and stress-strain plots for the differently prepared hydrogels. According to the results obtained, the compressive strength measurement revealed a significant difference for the differently prepared hydrogels. This relates to the concentrations of GG and the CA used during the crosslinking process to form polymer-CA-polymer and polymer-CA-PEG-CA-polymer bonds [29, 50, 55]. GB3 showed the highest compression force used. This can be attributed to the high concentration of GG used, which increased the gel viscosity and intend its hardness. Contrary to that result, the control sample (GB0) shows the weakest compressibility. This phenomenon may be attributed to the size of BC, which after vigorously blending at 30000 rpm for 1 minute was not small enough

to allow full interaction of cellulose and gellan gum, resulting in limited compressibility of the prepared materials. On the other hand, GB0 showed great swelling as examined in section 3.2.

3.6. Thermogravimetric analysis (TGA)

The thermal stability of the investigated hydrogels is shown in Figure 3b. The obvious difference in the control sample (GB0) thermal curve was attributed to the absence of the crosslinking elements (CA and PEG). Considering the 5 crosslinked hydrogels, the first slight loss in weight from 25 - 110 °C is attributed to the loss of water moisture from the hydrogel network. The second weight loss phase observed in the temperature range from 160 to 380 °C with maximum decomposition is due to the degradation of polymer chains. During this stage, differences in the prepared hydrogels are observable. The variation in thermal stability at this phase may be related to the difference in the concentration of GG and the amount of crosslinking density. The different compositions cause changes in the structural network assembly, resulting in the difference in heat resistance of the hydrogels [34]. As observed from Figure 3b, GB3 hydrogel showed lower degradation as compared to the other hydrogels. This was as a result of the high concentration of GG in the hydrogel composition that increased hardness and density of the hydrogel network and thus higher thermal stability. Finally, the degradation phase above 350 °C relates to the formation of char residues for all prepared hydrogels.

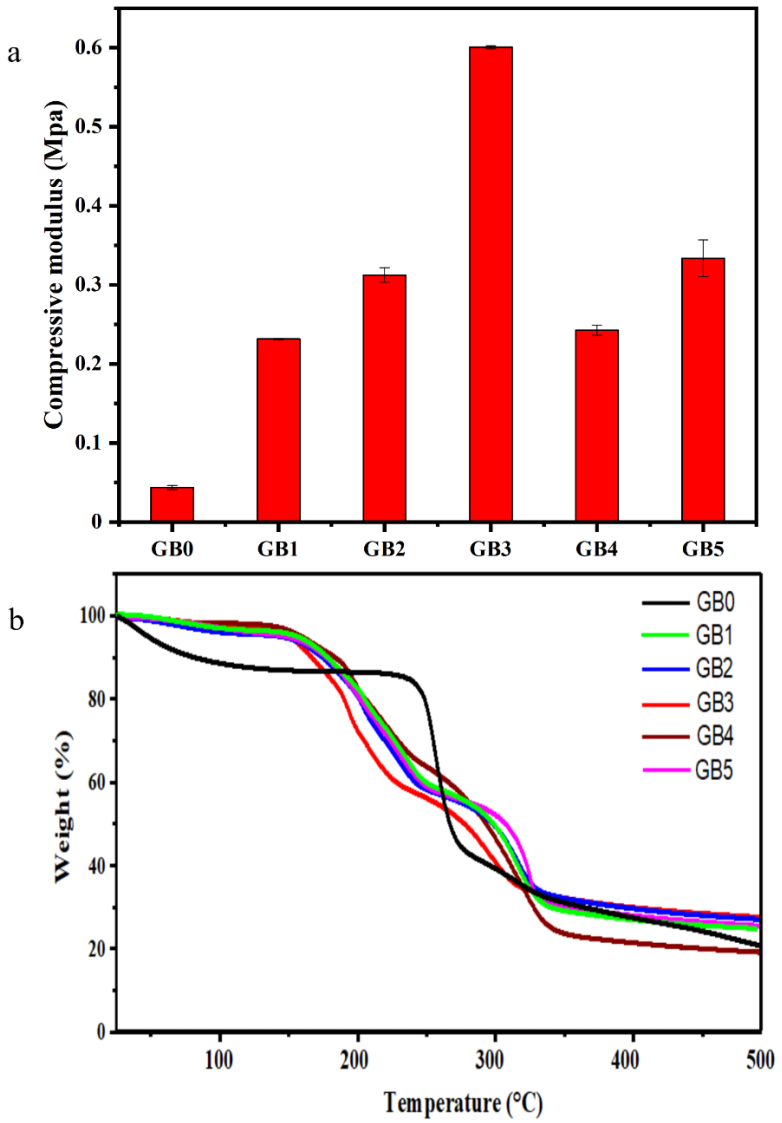

Fig. 3. a) Mechanical stability compressive modulus and b) thermograms of prepared GB hydrogels.

3.7. Surface morphology analysis by SEM

Figure 4 illustrates the cross-section morphology of the GB hydrogels investigated by SEM. The detailed analysis revealed a honeycomb-like network with the presence of large pores and channels of high interconnectivity. Although GG and BC were used in all the samples, their different concentrations and amounts of CA (crosslinking agent) influenced the porous architecture as revealed by the SEM images taken at varying magnifications (250x and 500x). Pores of ≈300 µm in size or larger and a multitude of pores between 50 - 200 µm were observed. Labyrinth chambers and channels with a narrow distribution of sizes wer also revealed by the SEM images. The large

pore size and thin wall layer in GB3 is probably due to the high amount of GG. Contrarily, the aggregated assembly structure in GB1 with narrower structure network may be related to the low amount of GG. However, the observed results depict the homogenous blending and crosslinking between BC, GG and PEG. Nevertheless, small differences in the pore size and the pore wall layer thickness in the micrographs were observed. This phenomenon may relate to the variation in concentrations of GG in the hydrogel materials. Similar hydrogel structures have also been reported by Salama et al. (2018) and Hua et al. (2021) [56, 57].

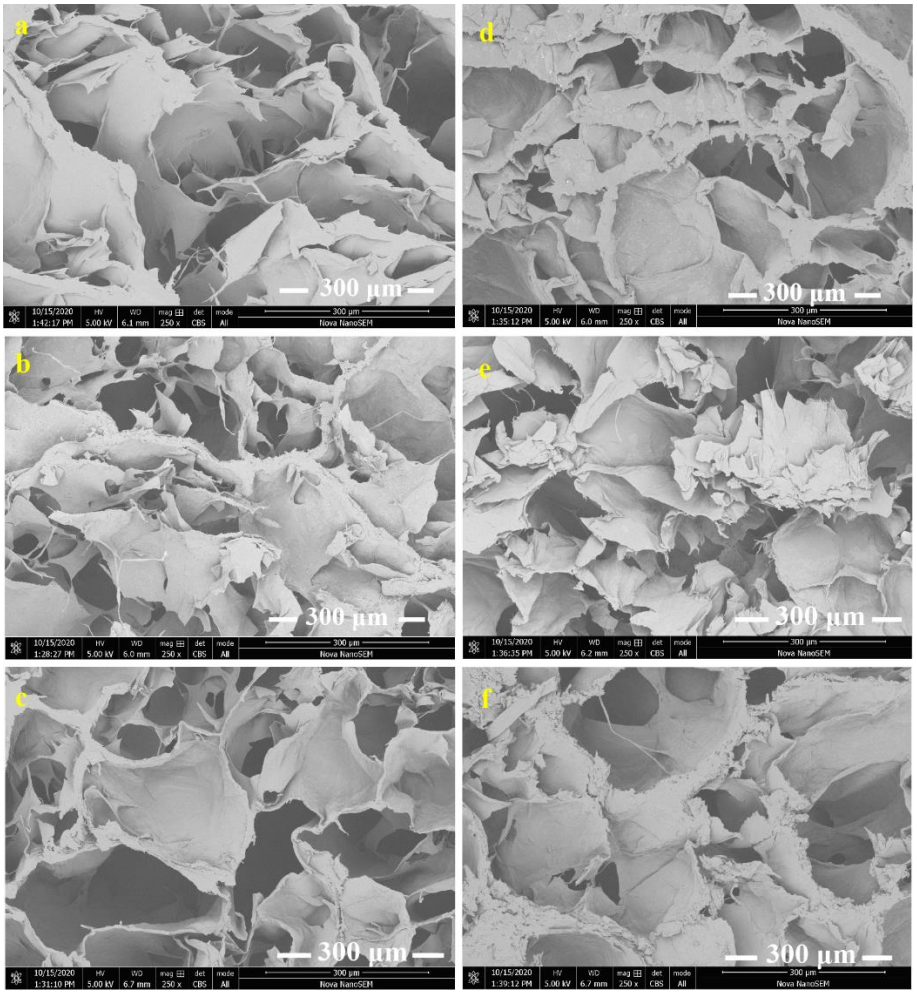

Fig. 4. SEM micrographs of the a) GB0, b) GB1, c) GB2, d) GB3, e) GB4 and f) GB5 hydrogels.

3.8. Batch adsorption analysis

Following the characterization and swelling behavior of the different hydrogels, the best-suited sample for further adsorption evaluation as the dye adsorbent was considered. As observed in Figure 1 and 3, despite the outstanding swelling capacity of GB0, its compression strength was the

lowest, which limits the material's shape stability and reusability performance. In contrast, the other samples showed considerable mechanical strength with GB4 being the most suitable considering its swelling capacity and mechanical stability. Thus, sample GB4 was selected as the best GB hydrogel sample for further adsorption studies by investigating the effect of contact time, solution pH, dye concentration, adsorbent dosage and temperature on its dye removal efficiency.

Figure 5a reveals the effect of contact time on the removal of SO and CV dyes in the range from 30 to 600 min. According to the results, the removal efficiency of the different dyes significantly increased between the first 30 to 60 min, followed by a gradual continuous increase to equilibrium. The rapid initial increase in the quantity of adsorbed dyes may be attributed to the high number of vacant sites available at the beginning of the adsorption, which gradually saturates with the increase in time. Similar effects were observed in a previous report by Riham et al. (2018) and Erdem et al. (2016) [42, 45].

Figure 5b illustrates the effect of solution pH on the adsorption of SO and CV from the aqueous phase. As observed, the dye removal efficiency was maximum at pH 7 for SO and CV determined as 58.29% and 28.20%, respectively. The higher removal efficiency achieved for SO as compared to CV dye, illustrates the higher binding affinity of SO to GB hydrogel. To further explain the impact of pH on SO and CV adsorption, the removal efficiency increases from pH 3 to 7 and then followed a gradual decrease to pH 11. In acidic pH, a decrease in removal capacity was observed for both dyes. The lower adsorption at acidic pH is attributed to the presence of excess H^+ ions competing with the dye cations. Conversely, at alkali pH ($pH \geq 7$), the hydrogel surface is more negatively charged, facilitating interaction between the cationic dyes and the adsorbent surface. However, the higher values of adsorption obtained at pH 7 as compared to pH>7 suggest that the adsorption of the dyes on the hydrogels was more favored by hydrogen bonds and van der Waals forces rather than electrostatic interactions [15, 24, 40, 45].

Figure 5c shows the removal efficacy of GB hydrogel in different concentrations of SO and CV dyes from 1 to 10 mg/L. The percentage of dye removal decreased with increasing the dye concentrations. This can be related to the decrease in the number of active sites of the GB hydrogel at higher dye concentrations. Contrarily, the adsorption capacity increases with increasing the dye concentration, which is attributed to the difference in the concentration gradient. This creates a

sufficient driving force for the dye molecules to overcome mass transfer resistance between the solid and liquid phases in the hydrogel porous channels. Similar results have been reported by Riham et al. (2018), Erdem et al. (2016), and Zhou et al. (2014), [40, 42, 45].

Figure 5d presents the effect of adsorbent dosage on the dye removal capacity of SO and CV, which increased with increasing dosage from 100 to 300 mg. It is easy to explain this result on the basis of the differences in the number of active groups and diffusion path lengths that were contained on the surface and within the hydrogel [42]. By increasing the dosage of the adsorbent, the number of available active sites increases which led to an increase in dye adsorption. Ultimately, a large number of adsorption sites increases interaction with the dye molecules.

Figure 5e shows the effect of temperature on the adsorption of SO and CV in the range of 25 to 55 °C. As revealed, the optimum removal efficacy of the dyes was achieved at 25 °C. It can be inferred that the adsorption process is slightly endothermic. Although the collisions between the dye molecules and hydrogel increase with temperature, some undesired reactions may have occurred at higher temperature thereby causing dissolution or shortening of molecular chains. This could have affected the hydrogel network structure leading to a reduction in swelling and in tend dye removal capacity [40, 45].

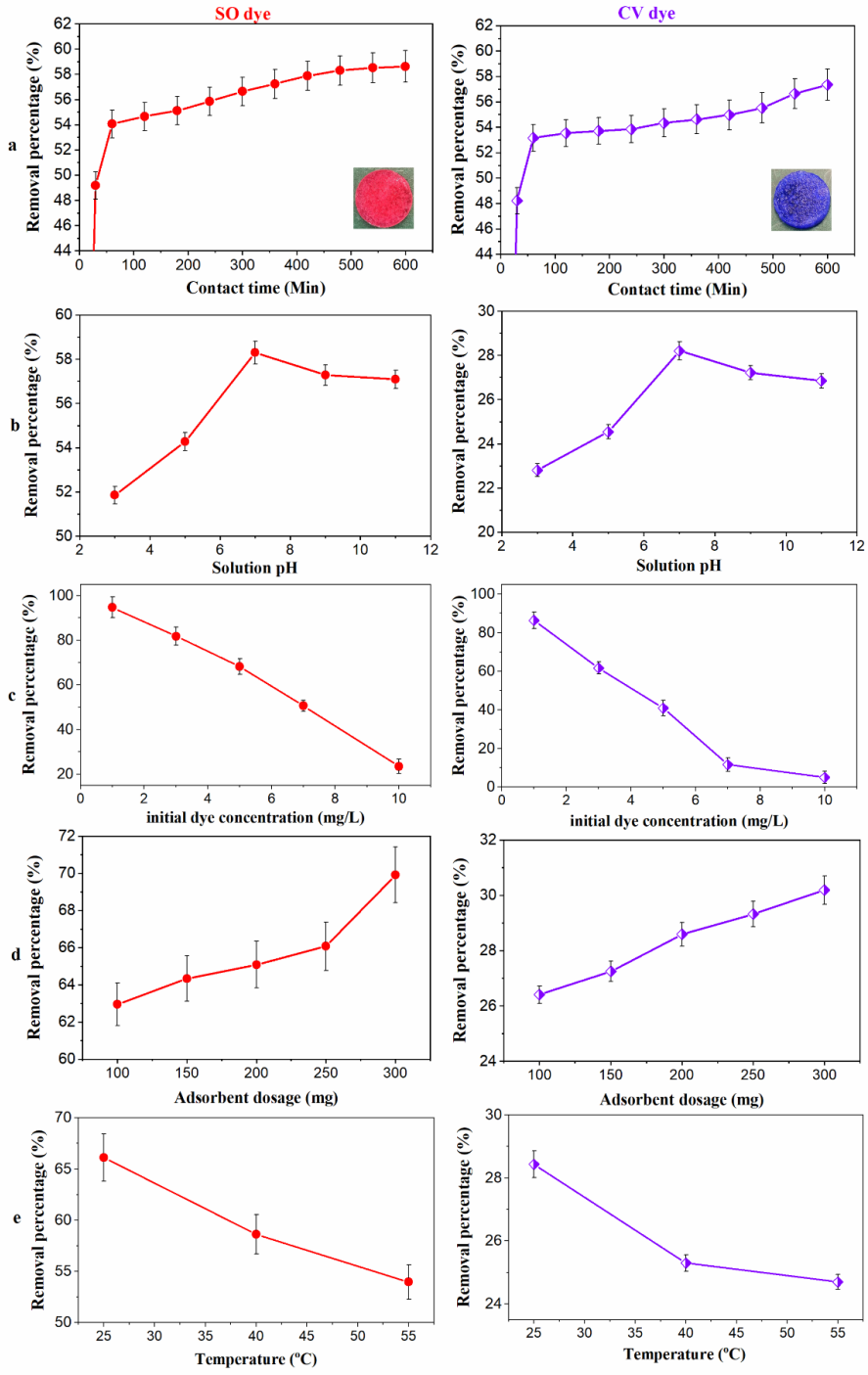

Fig. 5. Effects of different adsorption parameters: a) contact time, b) solution pH, c) initial dye concentration, d) adsorbent dosage and e) temperature on the removal of SO and CV dyes using GB hydrogel.

3.9. Point zero charge (PZC) and adsorption mechanism

To further explain the impact of pH and the mechanism of dye removal, the PZC of GB hydrogel was studied and discussed. As can be seen in Figure 6a, the obtained PZC of the GB hydrogel was determined at pH_{pzc} = 6.0. According to literature, under PZC value, the surface of the absorbent becomes positively charged while above this value, the material surface acquired a negative charge [58, 59]. However, the higher values of adsorption obtained at neutral pH as compared to pH_{pzc} suggest that the adsorption of the dyes on GB hydrogel might be more favored by hydrogen bonds and van der Waals forces than electrostatic interactions [17, 24].

The proposed mechanism for the adsorption of SO and CV dyes onto GB hydrogel is shown in Figure 6b. The adsorbent active groups consisting of –OH or –COO groups are the focal points that bound to cyclic functional groups containing radicals such as amine or sulfurize groups in SO and CV dyes. Herein, the change in structural composition due to the interaction with dye particles in the post-adsorbed materials (GB-CV and GB-SO) depicted at least three different spectra peaks when compared to the spectra of the non-adsorbed hydrogel (Figure 6c(i)). The changes in magnitude and sharpness of the bands around 3025 -3070, 1725, and 1040 – 1150 cm^{-1} were attributed to the increase in bond interactions of C=O, C-H, C-O-C groups with the dye molecules. In addition, the almost disappearing band at 890 which is characteristic for GG in GB-CV and GB-SO spectra revealed a weakness in the frequency of occurrence of the CH group. A further confirmed by SEM micrographs of the post-adsorbed hydrogels is shown in Figure 6c(ii). Numerous dye particles randomly attached to the surface of the hydrogels were observed.

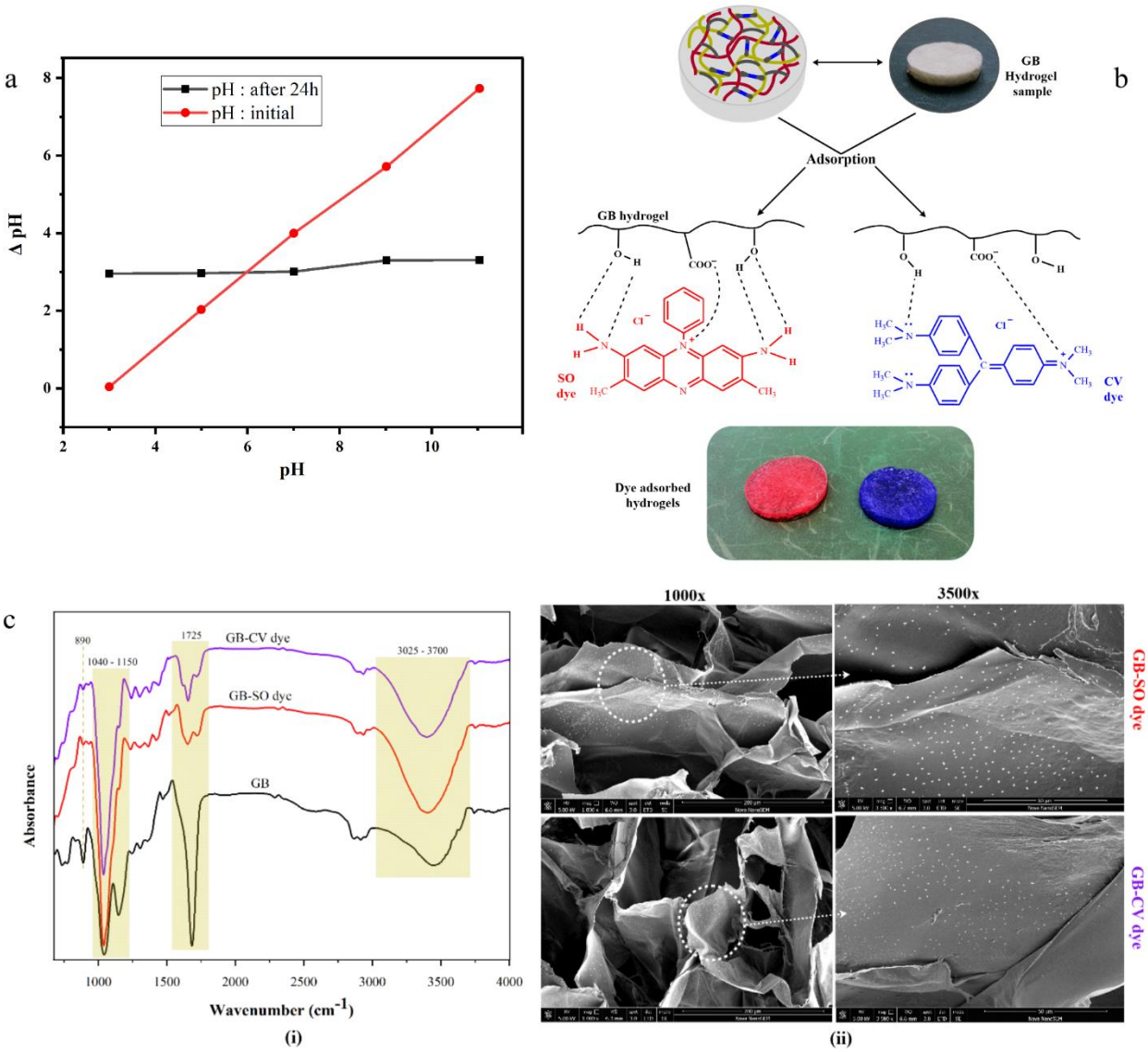

Fig. 6. a) PZC determination of GB hydrogel. b) Proposed mechanism for the adsorption of SO and CV dyes onto GB hydrogel and c) (i.) FTIR and (ii.) SEM image confirming the binding and adsorption of the dye molecules onto the adsorbent at 1000x and 3500x magnifications.

3.10. Adsorption kinetics, isotherm modeling and thermodynamics

Based on the Pseudo-1st order equation, a plot of *log* (Q_e-Q_t) versus *t* (Figure 7a) was deduced and the values of K_1 and Q_e were obtained from the slope and intercept, respectively. A graph of *t/qt* versus *t* (Figure 7b) was also plotted based on the pseudo-2nd order model to determine the values of K_2 and Q_e from the slope and intercept, respectively. A plot of Q_t versus $t^{0.5}$ (Figure 7c) for the intraparticle diffusion model was plotted to determine K_3 and *C*. A plot of *Bt* versus *t* (Figure 7d) was plotted for Boyd model. The results revealed a low correlation fit between the experimental

and calculated data for the pseudo-1st order model (SO dye R^2 = 0.901 and CV dye R^2 = 0.802), while the data was well described by the pseudo-2nd order model (SO dye R^2 = 0.999 and CV dye R^2 = 0.997) as provided in Table 2. In addition, other error analysis parameters such as a sum of squared error (SSE) and reduced chi-squared (χ^2) values were comparatively lower than that of the pseudo-1st order kinetic model. This confirms the adsorption of SO and CV dyes onto GB hydrogel best fitted the pseudo-2nd order kinetic model [1, 5, 8, 60, 61]. The intraparticle diffusion model showed three regions; step 1 film diffusion, which relates to the quick adsorption of dye molecules from the aqueous phase to the boundary layer of the hydrogel, step 2 gradual adsorptions that correspond to the diffusion of dye molecules within the porous sites of the hydrogel and step 3 equilibrium phase relates to the adsorption of dye molecules on the interior surface of the hydrogel. The presence of three adsorption stages (Figure 7c) with non-zero intercepts of C (thickness of the boundary layer) = 1.28 and 1.26 mg/g for SO and CV, respectively (Table 2), suggests intraparticle diffusion participates as the rate limiting step. High R^2 values of 0.986 and 0.895 determined for SO and CV dye adsorption, respectively, depicted the intraparticle diffusion model well described the adsorption mechanism of the dye molecules onto the investigated adsorbent. This was further supported by the Boyd model which did pass through the origin (Figure 7d), confirming intraparticle diffusion as the rate-limiting step [41, 44, 45].

Figure 7b depicts the adsorption isotherms fitted to Langmuir and Freundlich isotherm models. The Langmuir and Freundlich equilibrium parameters and their corresponding fitting correlation coefficients (R^2). The deduced results showed high R^2 values for Langmuir (R^2 = 0.999 for SO and 0.987 for CV) and Freundlich (R^2 = 0.997 for SO and 0.985 for CV) isotherm models (Table 2). The Langmuir maximum adsorption capacities (Q_m) were determined as 17.57 and 13.49 mg/g for SO and CV dye, respectively, suggesting that the adsorption of the dyes occurred more preferably via monolayer than heterogeneous formation. K_L was deduced as 1.78 x 10^{-2} and 2.46 x 10^{-3} for SO and CV dye, respectively. R_L, the dimensionless separation factor was in the range of 0.848 – 0.997, indicating the adsorption process of SO and CV onto GB hydrogel was favorable. On the other hand, the values of 1/n from Freundlich isotherm model were determined as 0.739 and 0.934 for SO and CV dye (Table 2), respectively, which is less than 1, indicating GB hydrogel was a suitable adsorbent for the removal the dyes.

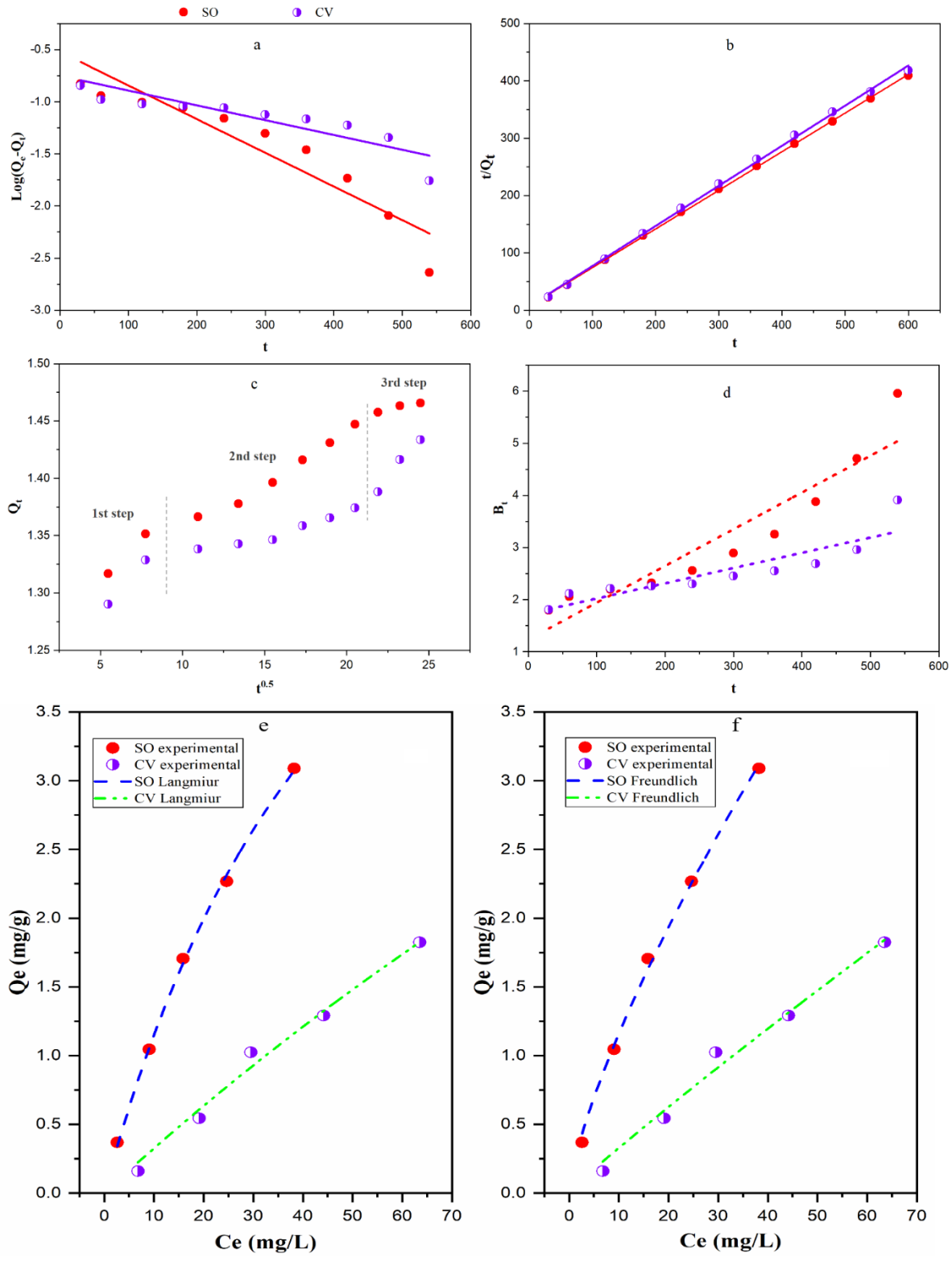

Fig. 7 Adsorption kinetic models of a) pseudo 1st-order and b) pseudo 2nd-order, c) intraparticle diffusion and d) Boyd model. Regression plots of e) Langmuir and f) Freundlich isotherm models for the adsorption of SO and CV dyes onto GB hydrogel.

Table 2.
Parametric values of kinetics and isothermic models for SO and CV dye removal of investigated GB hydrogel adsorbent.

Kinetic models	**Parameter**	**SO**	**CV**
Pseudo 1st-order	$Q_{e,cal}$ (mg.g^{-1})	0.301	0.177
	$Q_{e,expt}$ (mg.g^{-1})	1.465	1.434
	K_1 (min^{-1})	7.45 x 10^{-3}	3.27 x 10^{-3}
	R^2	0.901	0.802
	SSE	0.041	0.017
	χ^2	0.324	0.140
Pseudo-2nd order	$Q_{e,cal}$ (mg.g^{-1})	1.484	1.430
	$Q_{e,expt}$ (mg.g^{-1})	1.465	1.434
	K_2 (g.mg^{-1}.min^{-1})	6.51 x 10^{-2}	6.78 x 10^{-2}
	R^2	0.999	0.997
	SSE	0.005	0.002
	χ^2	0.058	0.021
Intraparticle diffusion	C (mg.g^{-1})	1.28	1.26
	K_p (g.mg^{-1}.min$^{-1/2}$)	3.12 x 10^{-4}	6.86 x 10^{-4}
	R^2	0.986	0.895
	SSE	3.51 x 10^{-4}	1.70 x 10^{-3}
	χ^2	3.89 x 10^{-5}	1.88 x 10^{-4}
Boyd	R^2	0.938	0.890
	SSE	1.889	0.626
	χ^2	0.236	0.078

Isotherm models						
Langmuir						
	Q_m (mg/g)	**K_L (L/mg)**	**R_L**	**R^2**	**SSE**	**χ^2**
SO	17.57	1.78 x 10^{-2}	0.848 – 0.982	0.999	0.521	0.0014
CV	13.49	2.46 x 10^{-3}	0.975 – 0.997	0.987	1.031	0.0071
Freundlich						
	K_F (mg/g)(L/mg)		**1/n**	**R^2**	**SSE**	**χ^2**
SO	21.06 x 10^{-2}		0.739	0.997	0.022	0.0041
CV	3.81 x 10^{-2}		0.934	0.985	0.013	0.0081

The study on the influence of temperature change on the adsorption process is very vital for describing the insights about its nature. ΔG° describes the spontaneity of the adsorption system

and the more negative the values, the more favorable the adsorption process. According to the results obtained (Table 3), ΔG° values for the adsorption process revealed that SO dye adsorption process on the surface of the GB hydrogel was spontaneous, reversible and more favorable than CV. Both ΔH^o and ΔS^o values for the two dyes adsorption were calculated from the slope and intercept of the linear Van't Hoff plot (Figure 8a) and listed in Table 3. This table also depicts that the negative values of ΔH^o for both dyes confirm the exothermic nature of the adsorption process. While, the negative ΔS^o values for both dyes relate to the decrease in randomness at the solid/liquid interface during the adsorption process [24, 46, 60].

Table 3.
Thermodynamic values for the adsorption of SO and CV dyes onto GB hydrogel.

Thermodynamics						
Parameters	**Temperature**					
	SO			**CV**		
	298 K	313 K	328 K	298 K	313 K	328 K
ΔG° (kJ/mol)	-1.636	-0.952	0.407	2.310	2.766	3.077
ΔH° (kJ/mol)		-13.866			-5.241	
ΔS° (J/mol K)		-41.110			-25.416	

3.11. Reusability study

The reusability evaluation of adsorbents has been widely considered essential to inspect their economic feasibility and practical application potential [1, 62]. To this effect, adsorption-desorption cycles as described in Section 2.7 use dH_2O at 60 °C as an eluent and HCl as the regeneration solution [40, 62]. Figure 8b shows the reusability ability of the GB hydrogel for 5 cycles. As observed, the adsorption efficiency of the hydrogel for both SO and CV dye revealed high stability in retaining their removal capacity within the studied cycles with a low loss in performance capacity (under 2%). These results might be attributed to the mechanical robustness and stability of the examined adsorbents [5]. In addition, the recovery percentage of the dyes from the adsorbents after desorption was more than 95%. This promoted the recognition that the GB hydrogel possesses good regeneration properties for a minimum of 5 cycles and could be identified as an adsorbent for cationic and anionic dye removal in contaminated textile dye water.

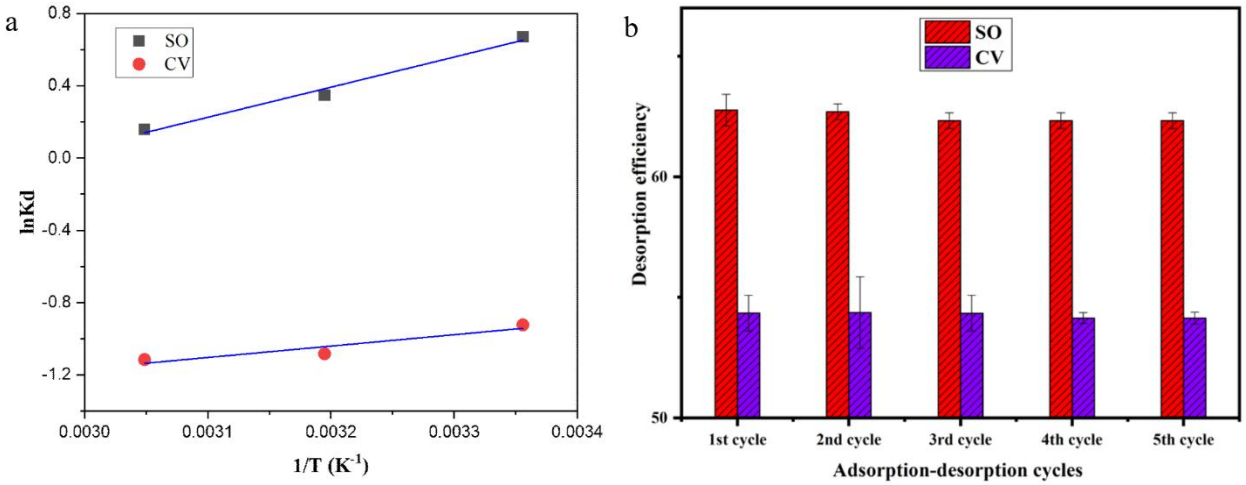

Fig. 8. a) Van't Hoff plots for the removal of SO and CV dyes and b) reusable cycles for GB hydrogel as an adsorbent.

3.12. Comparison to other adsorbents

The maximum adsorption capacities of SO and CV dyes for GB hydrogel were compared to data reported in previous similar studies (Table 2). It is very clear that the absorption efficiency of GB hydrogel is superior to some previous studies and shows its promising potential as a suitable material for water treatment.

Table 4.
Comparison for the adsorption of SO and CV dyes with various reported adsorbents.

Adsorbent materials	Dye solutions (mg/L)	Solution pH	Max. adsorption (mg/g)	Ref
Shells of Sepia pharaonis/Urea	CV	10.6	0.536	[62]
Clay/poly(N-isopropylacrylamide) nanocomposite	CV	8.9	7.6	[11]
Sodium alginate/gelatin based ZnS-nanocomposite	CV	9	9.32	[61]
Gellan gum/acrylamide/poly(vinyl alcohol	CV	7	45.5	[63]
Nanomagnetic iron oxide	CV	9	16.5	[14]
Magnetic κ-carrageenan-g-poly(methacrylicacid) nanocomposite	CV	7	28.24	[46]

Acrylamide/sodiumalginate/2-acrylamido-2-methylpropane sulphonic acid	CV	6.8	3.34	[58]
Phosphoric acid-treated coconut coir	SO	6	96.81	[64]
Kaolinite/Clay	SO	9	16.23	[65]
Pineapple peel wastes	SO	6	21.7	[66]
Alkaline-treated rice husk	SO	5.5	9.77	[67]
Gellan gum/bacterial cellulose	SO	7	17.57	**This study**
Gellan gum/bacterial cellulose	CV	7	13.49	**This study**

4. Conclusions

The decontamination of water pollutants is of great importance for the better well-being of humans, animals and aquatic organism development. In this study, the preparation of green adsorbents based on the crosslinking of GG and BC using CA was successfully explored. The developed adsorbent was investigated for its adsorption efficacy, and it demonstrated efficiency in the uptake of SO and CV dyes. The adsorption process was described as exothermic and well-fitted Langmuir model and pseudo 2nd-order kinetic. After five adsorption-desorption cycles, the investigated dye removal capacity of the GB hydrogel remained approximately constant. However, the adsorption capacities of SO and CV dyes using the prepared hydrogel were not significantly high accompanied by a high secondary pollution risk of desorbed solvent (HCl solution). As such, further experiments are evidently required to optimize the performance of this adsorbent hydrogel for improvements in terms of economic and large-scale feasibility.

In summary, BC produced from bio-waste (sour whey waste) in this study shows a huge potential for the use of low-cost BC sources in the preparation of green adsorbents for water remediation purposes to take dual benefit in environmental protection (processing bio-waste liquid into a useful material to treat other pollutant liquid). Furthermore, the cost of BC source is currently high. However, the hydrogel preparation approach in this work with the incorporation of GG helps mitigates the cost of the BC-based adsorbent as an effort to improve the competitiveness with other adsorbents in the market.

Acknowledgments

This work is supported by the Ministry of Education, Youth and Sports of the Czech Republic – DKRVO (RP/CPS/2022/005) and Internal grant (project: IGA/CPS/2020/005 and IGA/CPS/2021/002) from Tomas Bata University in Zlin, Czech Republic.

Author Contributions

Conceptualization and methodology was performed by Hau Trung Nguyen and Fahanwi Asabuwa Ngwabebhoh. Formal analysis and investigation by Hau Trung Nguyen. Data curation was done by Hau Trung Nguyen and Fahanwi Asabuwa Ngwabebhoh. Writing-original draft preparation, Hau Trung Nguyen. Writing-review and editing by Nabanita Saha and Fahanwi Asabuwa Ngwabebhoh. Supervision Nabanita Saha. Funding acquisition by Tomas Saha and Petr Saha. All authors have read and agreed to the published version of the manuscript.

Conflict of Interest Statement

The authors declare no conflict of interest in the present study.

Informed consent statement

The nutrient sources of waste whey collected from Kromilk A. S. were used with informed consent and permission from the responsible authorities of the company.

References

[1] X.G. Huang, X.Z. Zhan, C.L. Wen, F. Xu, L.J. Luo, Amino-functionalized magnetic bacterial cellulose/activated carbon composite for Pb2+ and methyl orange sorption from aqueous solution, Journal of Materials Science & Technology 34(5) (2018) 855-863.

[2] X. Chen, J. Cui, X.R. Xu, B.J. Sun, L. Zhang, W. Dong, C.T. Chen, D.P. Sun, Bacterial cellulose/attapulgite magnetic composites as an efficient adsorbent for heavy metal ions and dye treatment, Carbohydrate Polymers 229 (2020) 115512.

[3] E.P. Ferreira-Neto, S. Ullah, T.C.A. da Silva, R.R. Domeneguetti, A.P. Perissinotto, F.S. de Vicente, U.P. Rodrigues, S.J.L. Ribeiro, Bacterial nanocellulose/MoS2 hybrid aerogels as bifunctional adsorbent/photocatalyst membranes for in-flow water decontamination, ACS Applied Materials & Interfaces 12(37) (2020) 41627-41643.

[4] L. Males, D. Fakin, M. Bracic, S. Gorgieva, Efficiency of differently processed membranes based on cellulose as cationic dye adsorbents, Nanomaterials 10(4) (2020) 642.

[5] Y. Hu, C.T. Chen, L.Y. Yang, J. Cui, Q.L. Hao, D.P. Sun, Handy purifier based on bacterial cellulose and Ca-montmorillonite composites for efficient removal of dyes and antibiotics, Carbohydrate Polymers 222 (2019) 115017.

[6] F.J.L. Ferreira, L.S. Silva, M.S. da Silva, J.A. Osajima, A.B. Meneguina, S.H. Santagneli, H.S. Barud, R.D.S. Bezerra, E.C. Silva, Understanding kinetics and thermodynamics of the interactions between amitriptyline or eosin yellow and aminosilane-modified cellulose, Carbohydrate Polymers 228 (2020) 115246.

[7] M. Rafatullah, O. Sulaiman, R. Hashim, A. Ahmad, Adsorption of methylene blue on low-cost adsorbents: A review, Journal of Hazardous Materials 177(1-3) (2010) 70-80.

[8] Z.H. Wang, B. Xiang, R.M. Cheng, Y.J. Li, Behaviors and mechanism of acid dyes sorption onto diethylenetriamine-modified native and enzymatic hydrolysis starch, Journal of Hazardous Materials 183(1-3) (2010) 224-232.

[9] Y. Hu, F. Liu, Y.B. Sun, X.R. Xu, X. Chen, B.C. Pan, D.P. Sun, J.S. Qian, Bacterial cellulose derived paper-like purifier with multifunctionality for water decontamination, Chemical Engineering Journal 371 (2019) 730-737.

[10] Y. Seida, H.J.G. Tokuyama, Hydrogel adsorbents for the removal of hazardous pollutants—requirements and available functions as adsorbent, Gels 8(4) (2022) 220.

[11] Q.S. Zhang, T.T. Zhang, T. He, L. Chen, Removal of crystal violet by clay/PNIPAm nanocomposite hydrogels with various clay contents, Applied Clay Science 90 (2014) 1-5.

[12] L.M. Zhang, Y.J. Zhou, Y. Wang, Novel hydrogel composite for the removal of water-soluble cationic dye, Journal of Chemical Technology Biotechnology 81(5) (2006) 799-804.

[13] P.P.S. Ambika, Natural polymer-based hydrogels for adsorption applications, Natural Polymers–Based Green Adsorbents for Water Treatment 267 (2021) 267-306.

[14] S. Hamidzadeh, M. Torabbeigi, S.J. Shahtaheri, Removal of crystal violet from water by magnetically modified activated carbon and nanomagnetic iron oxide, Journal of Environmental Health Science and Engineering 13 (2015) 1-7.

[15] M. Zheng, K. Cai, M. Chen, Y. Zhu, L. Zhang, B. Zheng, pH-responsive poly(gellan gum-co-acrylamide-co-acrylic acid) hydrogel: Synthesis, and its application for organic dye removal, International Journal of Biological Macromolecules 153 (2020) 573-582.

[16] S.A. Zauro, B. Vishalakshi, Amphoteric gellan gum-based terpolymer–montmorillonite composite: synthesis, swelling, and dye adsorption studies, International Journal of Industrial Chemistry 8(3) (2017) 345-362.

[17] M. Zheng, K. Cai, M. Chen, Y. Zhu, L. Zhang, B. Zheng, pH-responsive poly (gellan gum-co-acrylamide-co-acrylic acid) hydrogel: Synthesis, and its application for organic dye removal, International Journal of Biological Macromolecules 153 (2020) 573-582.

[18] C. Modrogan, A.M. Pandele, C. Bobirică, D. Dobrotă, A.M. Dăncilă, G. Gârleanu, O.D. Orbuleţ, C. Borda, D. Gârleanu, C. Orbeci, Synthesis, characterization and sorption capacity examination for a novel hydrogel composite based on Gellan gum and Graphene oxide (GG/GO), Polymers 12(5) (2020) 1182.

[19] J.S. Karthika, B. Vishalakshi, Novel stimuli responsive gellan gum-graft-poly(DMAEMA) hydrogel as adsorbent for anionic dye, International Journal of Biological Macromolecules 81 (2015) 648-655.

[20] P. Ramburrun, P. Kumar, Y.E. Choonara, L.C. du Toit, V. Pillay, Design and characterization of neurodurable gellan-xanthan pH-responsive hydrogels for controlled drug delivery, Expert Opinion on Drug Delivery 14(3) (2017) 291-306.

[21] S. Hokkanen, A. Bhatnagar, M. Sillanpaa, A review on modification methods to cellulose-based adsorbents to improve adsorption capacity, Water Research 91 (2016) 156-173.

[22] R.E. Abouzeid, R. Khiari, N. El-Wakil, A. Dufresne, Current state and new trends in the use of cellulose nanomaterials for wastewater treatment, Biomacromolecules 20(2) (2019) 573-597.

[23] T.R. Stumpf, X.Y. Yang, J.C. Zhang, X.D. Cao, In situ and ex situ modifications of bacterial cellulose for applications in tissue engineering, Materials Science & Engineering C-Materials for Biological Applications 82 (2018) 372-383.

[24] D.Y. Yu, Y.J. Wang, M.H. Wu, L. Zhang, L.L. Wang, H.G. Ni, Surface functionalization of cellulose with hyperbranched polyamide for efficient adsorption of organic dyes and heavy metals, Journal of Cleaner Production 232 (2019) 774-783.

[25] W.L. Hu, S.Y. Chen, J.X. Yang, Z. Li, H.P. Wang, Functionalized bacterial cellulose derivatives and nanocomposites, Carbohydrate Polymers 101 (2014) 1043-1060.

[26] M.-T. Luo, H.-L. Li, C. Huang, H.-R. Zhang, L. Xiong, X.-F. Chen, X.-D. Chen, Cellulose-based absorbent production from bacterial cellulose and acrylic acid: synthesis and performance, Polymers 10(7) (2018) 702.

[27] L. Shen, H.L. Xu, L.J. Kong, Y.Q. Yang, Non-Toxic crosslinking of starch using polycarboxylic acids: kinetic study and quantitative correlation of mechanical properties and crosslinking degrees, Journal of Polymers and the Environment 23(4) (2015) 588-594.

[28] D. Nataraj, R. Reddy, N. Reddy, Crosslinking electrospun poly (vinyl) alcohol fibers with citric acid to impart aqueous stability for medical applications, European Polymer Journal 124 (2020) 109484.

[29] S.I. Swapnil, N. Datta, M.M. Mahmud, R.A. Jahan, M.T. Arafat, Morphology, mechanical, and physical properties of wet-spun cellulose acetate fiber in different solvent-coagulant systems and in-situ crosslinked environment, Journal of Applied Polymer Science 138(18) (2021) e50358.

[30] N. Reddy, Y.Q. Yang, Citric acid cross-linking of starch films, Food Chem. 118(3) (2010) 702-711.

[31] R. Salihu, S.I. Abd Razak, N.A. Zawawi, M.R.A. Kadir, N.I. Ismail, N. Jusoh, M.R. Mohamad, N.H.M. Nayan, Citric acid: A green cross-linker of biomaterials for biomedical applications, European Polymer Journal 146 (2021) 110271.

[32] V.S. Ghorpade, A.V. Yadav, R.J. Dias, K.K. Mali, S.S. Pargaonkar, P.V. Shinde, N.S. Dhane, Citric acid crosslinked carboxymethylcellulose-poly(ethylene glycol) hydrogel films for delivery of poorly soluble drugs, International Journal of Biological Macromolecules 18 (2018) 783-791.

[33] M. Hassan, N. Tucker, M.J. Le Guen, Thermal, mechanical and viscoelastic properties of citric acid-crosslinked starch/cellulose composite foams, Carbohydrate Polymers 230 (2020) 115675.

[34] D. Franklin, S. Guhanathan, Synthesis and characterization of citric acid-based pH-sensitive biopolymeric hydrogels, Polymer Bulletin 71(1) (2014) 93-110.

[35] R. Salihu, S.I. Abd Razak, N.A. Zawawi, M.R.A. Kadir, N.I. Ismail, N. Jusoh, M.R. Mohamad, N.H.M. Nayan, Citric acid: A green cross-linker of biomaterials for biomedical applications, European Polymer Journal (2021) 110271.

[36] F.A. Ngwabebhoh, N. Saha, H.T. Nguyen, U.V. Brodnjak, T. Saha, A. Lengalova, P. Saha, Preparation and characterization of nonwoven fibrous biocomposites for footwear components, Polymers 12(12) (2020) 3016.

[37] H.T. Nguyen, N. Saha, F.A. Ngwabebhoh, O. Zandraa, T. Saha, P. Saha, Kombucha-derived bacterial cellulose from diverse wastes: a prudent leather alternative, Cellulose 28(14) (2021) 9335-9353.

[38] T. Khampieng, S. Wongkittithavorn, S. Chaiarwut, P. Ekabutr, P. Pavasant, P. Supaphol, Silver nanoparticles-based hydrogel: characterization of material parameters for pressure ulcer dressing applications, Journal of Drug Delivery Science Technology 44 (2018) 91-100.

[39] D. Leal, W. De Borggraeve, M.V. Encinas, B. Matsuhiro, R. Müller, Preparation and characterization of hydrogels based on homopolymeric fractions of sodium alginate and PNIPAAm, Carbohydrate Polymers 92(1) (2013) 157-166.

[40] Y. Zhou, M. Zhang, X. Wang, Q. Huang, Y. Min, T. Ma, J. Niu, Removal of crystal violet by a novel cellulose-based adsorbent: comparison with native cellulose, Industrial Engineering Chemistry Research 53(13) (2014) 5498-5506.

[41] F.A. Ngwabebhoh, A. Erdem, U. Yildiz, Synergistic removal of Cu (II) and nitrazine yellow dye using an eco-friendly chitosan-montmorillonite hydrogel: Optimization by response surface methodology, Journal of Applied Polymer Science 133(29) (2016) 43664.

[42] R.R. Mohamed, M.H.A. Elella, M.W. Sabaa, G.R. Saad, Synthesis of an efficient adsorbent hydrogel based on biodegradable polymers for removing crystal violet dye from aqueous solution, Cellulose 25(11) (2018) 6513-6529.

[43] L. Saya, V. Malik, A. Singh, S. Singh, G. Gambhir, W.R. Singh, R. Chandra, S. Hooda, Guar gum based nanocomposites: Role in water purification through efficient removal of dyes and metal ions, Carbohydrate Polymers (2021) 117851.

[44] F.A. Ngwabebhoh, M. Gazi, A.A. Oladipo, Adsorptive removal of multi-azo dye from aqueous phase using a semi-IPN superabsorbent chitosan-starch hydrogel, Chemical Engineering Research Design 112 (2016) 274-288.

[45] A. Erdem, F.A. Ngwabebhoh, S. Çetintaş, D. Bingöl, U. Yildiz, Fabrication and characterization of novel macroporous jeffamine/diamino hexane cryogels for enhanced Cu (II) metal uptake: Optimization, isotherms, kinetics and thermodynamic studies, Chemical Engineering Research Design 117 (2017) 122-138.

[46] M. Gholami, M.T. Vardini, G.R. Mahdavinia, Investigation of the effect of magnetic particles on the crystal violet adsorption onto a novel nanocomposite based on κ-carrageenan-g-poly (methacrylic acid), Carbohydrate Polymers 136 (2016) 772-781.

[47] N. Reddy, Y. Yang, Citric acid cross-linking of starch films, Food Chemistry. 118(3) (2010) 702-711.

[48] A. Meftahi, R. Khajavi, A. Rashidi, M.K. Rahimi, A. Bahador, Preventing the collapse of 3D bacterial cellulose network via citric acid, Journal of Nanostructure in Chemistry 8(3) (2018) 311-320.

[49] S.I. Swapnil, N. Datta, M.M. Mahmud, R.A. Jahan, M.T. Arafat, Morphology, mechanical, and physical properties of wet-spun cellulose acetate fiber in different solvent-coagulant systems and in-situ crosslinked environment, Journal of Applied Polymer Science 138(18) (2021) 50358.

[50] N.S.V. Capanema, A.A.P. Mansur, A.C. de Jesus, S.M. Carvalho, L.C. de Oliveira, H.S. Mansur, Superabsorbent crosslinked carboxymethyl cellulose-PEG hydrogels for potential wound dressing applications, International Journal of Biological Macromolecules 106 (2018) 1218-1234.

[51] Z. Ma, Q. Li, Q. Yue, B. Gao, X. Xu, Q. Zhong, Synthesis and characterization of a novel super-absorbent based on wheat straw, Bioresource Technology 102(3) (2011) 2853-2858.

[52] D.M. Kirchmajer, Robust biopolymer based ionic–covalent entanglement hydrogels with reversible mechanical behaviour, Journal of Materials Chemistry B 2(29) (2014) 4694-4702.

[53] B. Tan, Z.H. Huang, Z.Y. Yin, X. Min, Y.G. Liu, X.W. Wu, M.H. Fang, Preparation and thermal properties of shape-stabilized composite phase change materials based on polyethylene glycol and porous carbon prepared from potato, RSC Advances 6(19) (2016) 15821-15830.

[54] E. Possenti, C. Conti, G.D. Gatta, M. Realini, C. Colombo, Diammonium hydrogenphosphate treatment on dolostone: the role of mg in the crystallization process, Coatings 9(3) (2019) 169.

[55] C. Chen, L. Wang, Y. Huang, Crosslinking of the electrospun polyethylene glycol/cellulose acetate composite fibers as shape-stabilized phase change materials, Materials Letters 63(5) (2009) 569-571.

[56] J. Hua, C. Liu, P.F. Ng, B. Fei, Bacterial cellulose reinforced double-network hydrogels for shape memory strand, Carbohydrate Polymers 259 (2021) 117737.

[57] A. Salama, Preparation of CMC-gP (SPMA) super adsorbent hydrogels: exploring their capacity for MB removal from waste water, International Journal of Biological Macromolecules 106 (2018) 940-946.

[58] T.U. Rehman, S. Bibi, M. Khan, I. Ali, L.A. Shah, A. Khan, M. Ateeq, Fabrication of stable superabsorbent hydrogels for successful removal of crystal violet from waste water, RSC Advances 9(68) (2019) 40051-40061.

[59] H. Mittal, P.P. Morajkar, A. Al Alili, S.M. Alhassan, In-Situ synthesis of ZnO nanoparticles using gum arabic based hydrogels as a self-template for effective malachite green dye adsorption, Journal of Polymers and the Environment 28(6) (2020) 1637-1653.

[60] H. Mittal, A. Al Alili, P.P. Morajkar, S.M. Alhassan, Graphene oxide crosslinked hydrogel nanocomposites of xanthan gum for the adsorption of crystal violet dye, Journal of Molecular Liquids 323 (2021) 115034.

[61] Priya, A.K. Sharma, B.S. Kaith, V. Tanwar, J.K. Bhatia, N. Sharma, S. Bajaj, S. Panchal, RSM-CCD optimized sodium alginate/gelatin based ZnS-nanocomposite hydrogel for the effective removal of biebrich scarlet and crystal violet dyes, International Journal of Biological Macromolecules 129 (2019) 214-226.

[62] K.Z. Elwakeel, A.M. Elgarahy, G.A. Elshoubaky, S.H. Mohammad, Microwave assist sorption of crystal violet and Congo red dyes onto amphoteric sorbent based on upcycled Sepia shells, Journal of Environmental Health Science and Engineering 18(1) (2020) 35-50.

[63] K. Arun Krishna, B. Vishalakshi, Gellan gum-based novel composite hydrogel: evaluation as adsorbent for cationic dyes, Journal of Applied Polymer Science 134(47) (2017) 45527.

[64] I. Ghosh, S. Kar, T. Chatterjee, N. Bar, S.K. Das, Adsorptive removal of Safranin-O dye from aqueous medium using coconut coir and its acid-treated forms: Adsorption study, scale-up design, MPR and GA-ANN modeling, Sustainable Chemistry Pharmacy 19 (2021) 100374.

[65] K.O. Adebowale, B.I. Olu-Owolabi, E.C. Chigbundu, Removal of safranin-O from aqueous solution by adsorption onto kaolinite clay, Journal of Encapsulation Adsorption Sciences 4(03) (2014) 89.

[66] M. Mohammed, A. Ibrahim, A. Shitu, Batch removal of hazardous safranin-O in wastewater using pineapple peels as an agricultural waste based adsorbent, International Journal of Environmental Monitoring Analysis 2(3) (2014) 128-133.

[67] S. Chowdhury, R. Misra, P. Kushwaha, P. Das, Optimum sorption isotherm by linear and nonlinear methods for safranin onto alkali-treated rice husk, Bioremediation Journal 15(2) (2011) 77-89.